
This is an electronic reprint of the original article.
This reprint may differ from the original in pagination and typographic detail.

Laurén, Isabella; Farzan, Afsoon; Teotia, Arun; Lindfors, Nina C.; Seppälä, Jukka

Direct ink writing of biocompatible chitosan/non-isocyanate polyurethane/cellulose nanofiber hydrogels for wound-healing applications

Published in:
International Journal of Biological Macromolecules

DOI:
[10.1016/j.ijbiomac.2024.129321](https://doi.org/10.1016/j.ijbiomac.2024.129321)

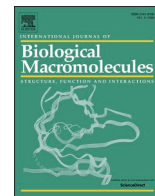
Published: 01/02/2024

Document Version
Publisher's PDF, also known as Version of record

Published under the following license:
CC BY

Please cite the original version:
Laurén, I., Farzan, A., Teotia, A., Lindfors, N. C., & Seppälä, J. (2024). Direct ink writing of biocompatible chitosan/non-isocyanate polyurethane/cellulose nanofiber hydrogels for wound-healing applications. *International Journal of Biological Macromolecules*, 259(Part 2), Article 129321. <https://doi.org/10.1016/j.ijbiomac.2024.129321>

This material is protected by copyright and other intellectual property rights, and duplication or sale of all or part of any of the repository collections is not permitted, except that material may be duplicated by you for your research use or educational purposes in electronic or print form. You must obtain permission for any other use. Electronic or print copies may not be offered, whether for sale or otherwise to anyone who is not an authorised user.



Direct ink writing of biocompatible chitosan/non-isocyanate polyurethane/cellulose nanofiber hydrogels for wound-healing applications

Isabella Laurén ^{a,1}, Afsoon Farzan ^{a,1}, Arun Teotia ^a, Nina C. Lindfors ^b, Jukka Seppälä ^{a,*}

^a Polymer Technology, School of Chemical Engineering, Aalto University, 02150 Espoo, Finland

^b Department of Hand Surgery, Helsinki University Hospital, University of Helsinki, 00290 Helsinki, Finland

ARTICLE INFO

Keywords:
Hydrogels
Chitosan
Wound-healing

ABSTRACT

The demand for new biocompatible and 3D printable materials for biomedical applications is on the rise. Ideally, such materials should exhibit either biodegradability or recyclability, possess antibacterial properties, and demonstrate remarkable biocompatibility with no cytotoxic effects. In this research, we synthesized biocompatible and 3D printable hydrogels tailored for biomedical applications, such as wound healing films, by combining antibacterial double-quaternized chitosan (DQC) with cystamine-based non-isocyanate polyurethane (NIPU-Cys) - a material renowned for enhancing both the flexibility and mechanical properties of the hydrogels. To improve the rheological behavior, swelling attributes, and printability, cellulose nanofibrils were introduced into the matrix. We investigated the impact of DQC on degradability, swelling capacity, rheological behavior, printability, and cell biocompatibility. The slightly cytotoxic nature associated with quaternary chitosan was evaluated, and the optimal concentration of DQC in the hydrogel was determined to ensure biocompatibility. The resulting hydrogels were found to be suitable materials for 3D printing via a direct ink writing technique (DIW), producing porous, biocompatible hydrogels endowed with valuable attributes suitable for various wound-healing applications.

1. Introduction

Due to their hydrophilic nature and biocompatibility, hydrogels have garnered significant attention for their exceptional properties, particularly in the biomedical field. These materials form porous 3D networks through polymer chains held together by chemical bonds or physical interactions, imparting them with desirable characteristics. The swelling capacity and morphology of hydrogels are crucial, impacting not only mechanical strength but also hydration capacity, diffusion, and internal transport properties [1–3]. Hydrogels, widely employed in biomedicine, especially in wound-healing applications, must facilitate easy removal and act as a barrier to prevent the entry of bacteria and impurities into the wound area. Tailoring materials to suit specific wounds is essential for effective healing, considering factors such as moisture control, exudate removal, gas transmission, biocompatibility, biodegradability, non-toxicity, and elasticity [4–6].

Polyurethanes (PUs), a versatile class of materials in various medical applications, are favored for their low cytotoxicity, suitable gas permeability, flexibility, and mechanical properties [7]. Typically

formed by reacting isocyanates with polyols, PUs pose challenges due to the highly toxic and flammable nature of isocyanates. Consequently, non-isocyanate PUs (NIPUs) have emerged as safer and more sustainable alternatives [8,9]. Given the hydrophilic nature of NIPUs [10], these polymers can form crosslinked networks with other hydrophilic materials like polysaccharides.

Commonly used in hydrogels due to their hydrophilic nature and exceptional biocompatibility, polysaccharides such as chitosan, alginates, and cellulose, play pivotal roles. Chitosan, with its low toxicity, biocompatibility, immune-stimulatory activities, antimicrobial properties, and adhesive nature, finds widespread use in various biomedical applications [11–13]. Various functional groups can be incorporated into its structure to enhance specific properties and address limitations, such as chitosan's aqueous solubility or antibacterial activity [14]. In prior studies, we introduced two distinct quaternary compounds, glycidyl trimethylammonium chloride (GTMAC) and [2-(Acryloyloxy)ethyl]-trimethylammonium chloride (AETMAC), into the chitosan structure to enhance its antimicrobial properties [15,16]. This heterogeneously double quaternized chitosan derivative (DQC) exhibits both

* Corresponding author.

E-mail address: jukka.seppala@aalto.fi (J. Seppälä).

¹ Equal contribution.

antiviral and antibacterial properties, making it a promising candidate for integration with other materials to create biocompatible hydrogels with proven antimicrobial efficacy.

By combining antimicrobial DQC with NIPU, we successfully produced viable and 3D-printable hydrogels with controlled micro- and macro-porous architecture. Careful assessment of DQC concentrations within the hydrogels mitigated potential cytotoxicity associated with quaternary chitosan - a crucial consideration depending on the targeted application. NIPU played a pivotal role as the main polymer matrix, enhancing the mechanical properties and flexibility of the printed structures. While PUs are conventionally used in molding processes, their adaptation to 3D printing presents challenges. To address this, TEMPO-oxidized cellulose nanofibrils (CNF) were introduced into the inks, enhancing the 3D printability and hydration behavior of the composite matrix. Furthermore, CNF significantly augmented hydrogen bonding between the components due to the abundance of hydroxyl groups on its surface. Our primary focus was synthesizing and characterizing the hydrogel inks for different physiochemical properties and printability. Further, these inks were used to 3D print porous scaffolds for *in vitro* assessments of the obtained hydrogels, marking an initial exploration of the potential application of DQC/NIPU/CNF hydrogels in biomedical contexts. Encouragingly, these hydrogels exhibited no acute harmful effects on fibroblast cells cultured on the scaffold surfaces, rendering them suitable as biocompatible barrier layers in various biomedical applications.

2. Experimental

2.1. Materials

Chitosan (CAS No. 9012-76-4, DDA \geq 75 %, M_w = 60 kDa) was purchased from TCI (Japan) and was used without further purification. GTMAC, AETMAC, ammonium persulfate (APS), 2-propanol, poly(ethylene glycol) diacrylate (PEGDA, M_n = 250), 1-thioglycerol (\geq 97 %), cystamine dihydrochloride (Cys, \geq 98 %), triethylamine (TEA, \geq 99.5 %), dimethyl sulfoxide (DMSO), potassium carbonate (K_2CO_3), 2,2-dimethoxy-2-phenyl-acetophenone (DMPA, 99 %), methanol, diethyl ether, dimethyl carbonate (DMC), Dulbecco's Modified Eagle Medium (DMEM) (cat no. D6429), penicillin (10,000 U/mL)-streptomycin (10 mg/mL) solution, trypsin-ethylenediaminetetraacetic acid (TE) (1 \times), fluorescein diacetate (FDA), propidium iodide (PI), and 3-(4,5-Dimethylthiazol-2-yl)-2,5-Diphenyltetrazolium Bromide (MTT) were purchased from Sigma-Aldrich (USA). Acetic acid (99–100 %) was purchased from VWR Chemicals (USA). Benzaldehyde (C_7H_6O), sodium hydroxide (NaOH), and sodium hydrogen carbonate ($NaHCO_3$) were obtained from Merck (Germany). TEMPO-CNF was obtained from our research group [17]. Fetal bovine serum (FBS) was purchased from Gibco/Thermo Fisher (USA).

2.2. Preparation of heterogeneously quaternized chitosan

To enhance both the solubility and the antimicrobial properties of chitosan, we introduced two kinds of quaternary ammonium compounds based on our prior research [15,16]. The reaction involved several steps. Initially, the amine groups of pure chitosan were reacted with benzaldehyde to exclusively introduce GTMAC to the *O*-position while avoiding unintentional reactions with the more reactive amine. For this step, 2.0 g chitosan was dissolved in 60 mL 2.0 wt% aqueous acetic acid and 40 mL methanol. After 1 h of stirring, 13.14 g benzaldehyde and 40 mL methanol were added, resulting in a highly viscous solution. The product was stirred for 24 h, followed by washing with acetone and subsequent freeze-drying. The dried chitosan was further washed with acetone for 30 min and treated with a 5.0 wt% aqueous solution of sodium hydrogen carbonate for 15 min. The resulting Schiff base chitosan (*N*-benzylidene-chitosan) was washed with distilled water, submerged in methanol for 12 h, and freeze-dried. The successful

preparation of Schiff base chitosan was confirmed by FT-IR, revealing the characteristic $C=N$ band at 1640 cm^{-1} (Fig. S1).

The obtained Schiff base chitosan was quaternized at the *O*-position with GTMAC. Here, 1.5 g (6.0 mmol) of the Schiff-base chitosan and 5.6 g (37.3 mmol) of GTMAC were dissolved in 75 mL 2-propanol and stirred for 30 h at 70 °C, followed by filtering, washing (1:1 acetone: ethanol), and freeze-drying. After successful quaternization of the hydroxyl group, the protected amine was deprotected to enable further quaternization at the *N*-position; the quaternized chitosan was suspended in 0.25 M HCl in ethanol overnight. The resulting single quaternized chitosan (SQC) was neutralized with NaOH, washed with ethanol, and freeze-dried. The final step involved the quaternization of SQC with AETMAC at the *N*-position, obtaining heterogeneously double quaternized chitosan (DQC). For this, 1.0 g of SQC was dissolved in 100 mL of 2 wt% acetic acid at 80 °C. Once fully dissolved, 1.0 g (4.4 mmol) of APS as an initiator and 2 mL (11.7 mmol) of AETMAC were gradually added and stirred for 3 h at 80 °C under an N_2 atmosphere. The resulting product was precipitated with acetone, repeatedly washed with methanol to remove any remaining poly-AETMAC and unreacted monomers, and finally freeze-dried. Successful polymerization was confirmed by 1H NMR and FT-IR (Scheme S1, Fig. S1). The degree of quaternization was determined as 1.3 according to 1H NMR spectra (Fig. S1), and the molecular weight was estimated to be 13 kDa, consistent with previous estimations [15].

2.3. Preparation of non-isocyanate polyurethane with a cystamine linker (NIPU-Cys)

NIPU-Cys was synthesized through a three-step reaction [18]. Tetraol was produced through a thiol-ene click (TEC) reaction involving PEGDA and 1-thioglycerol. Specifically, 90 mmol (20.25 mL) of PEGDA and 180 mmol (15.54 mL) of 1-thioglycerol were dissolved in 25 mL of methanol and stirred for 5 min at room temperature. Subsequently, 225 mg of DMPA was added as a photoinitiator, and the mixture was exposed to UV light ($\lambda = 365\text{ nm}$) for 45 min. The resulting viscose mixture was washed with diethyl ether and dried using a rotary evaporator. In the second step, 21 mmol (10 g) of the obtained tetraol was dissolved in 105 mmol (8.8 mL) of DMC and heated to 80 °C. Next, 290 mg of K_2CO_3 was introduced as a catalyst, and the mixture was stirred for 72 h. The synthesized bis(cyclic carbonate), appearing as a yellowish mixture, was precipitated in methanol, washed twice, and dried in a vacuum oven. In the third step, 19.2 mmol (10 g) of bis(cyclic carbonate), 19.2 mmol (2.92 g) of cystamine, and 38.4 mmol of TEA were dissolved in 38.5 mL of DMSO under an N_2 atmosphere. The temperature was raised to 100 °C and the mixture was stirred for 24 h. Finally, the viscose product was precipitated in acetone, washed twice to remove impurities, and stored in dark, sealed bottles. Successful preparation of NIPU-Cys was confirmed by 1H NMR and FT-IR analyses (Fig. S2).

2.4. Formation of DQC/NIPU-Cys/CNF hydrogels

The hydrogel composites were prepared with four different ratios of DQC incorporated into the NIPU-Cys-TEMPO-CNF matrix (Table 1) and utilized in 3D printing through a direct ink writing (DIW) technique. The concentration of DQC was adjusted within the range of 0–7.5 % (w/v) to investigate its impact on the biocompatibility and overall performance

Table 1
Ratios (%-w/v) used for the formation of DQC/NIPU-Cys/CNF hydrogel gels, containing various amounts of DQC.

Sample	DQC [%]	NIPU-Cys [%]	CNF [%]
HA	0	25	1.5
HB	2.5	25	1.5
HC	5	25	1.5
HD	7.5	25	1.5

of the hydrogel composite. NIPU-Cys was utilized to enhance the material's structure and provide a flexible and elastic matrix for the 3D scaffolds. Additionally, TEMPO-CNF (containing 1.5 wt% dry CNF [19]) was incorporated to improve 3D printability, swelling behavior, moisture retention, and to reinforce hydrogen bonding between the components (Scheme 1).

DQC and TEMPO-CNF were mixed until the DQC was fully dissolved in the TEMPO-CNF. Subsequently, NIPU-Cys was introduced to the solution, and given the hydrophilic nature of all components, the mixing procedure was conducted by gently using an electric homogenizer at low speed for 10 min. The gels were immediately printed after ink preparation using an extrusion-based DIW printing method. Printing parameters were meticulously adjusted through several cycles of material optimization, considering the rheological behavior of the inks, to ensure repeatability, dimensional accuracy, and stability of the printed structures. To preserve the structure and shape of the printed scaffolds, the materials were frozen in a freezer ($-18\text{ }^{\circ}\text{C}$) post-printing and subjected to freeze-drying for one day.

2.5. Characterization of the hydrogels

2.5.1. FT-IR spectroscopy

FT-IR spectra was determined with a Spectrum Two FT-IR spectrometer (PerkinElmer, UK). The samples were scanned in the range $4000\text{--}400\text{ cm}^{-1}$, with a resolution of 4 cm^{-1} and 64 accumulations, using an ATR setup equipped with a diamond window.

2.5.2. Thermogravimetric analysis (TGA)

TGA was conducted using a TA Q500 thermogravimetric analyzer (TA Instruments, USA). The heating range spanned from $30\text{ to }600\text{ }^{\circ}\text{C}$, with an increment of $10\text{ }^{\circ}\text{C}/\text{min}$ under N_2 flow.

2.5.3. ^1H NMR spectroscopy

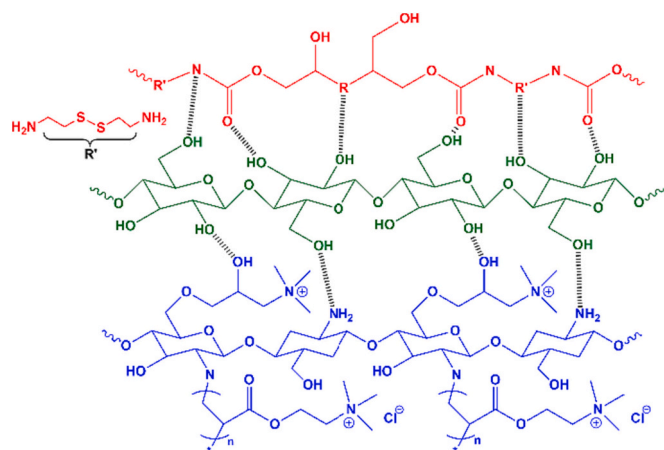
NMR analysis was performed with a Bruker III 400 MHz spectrometer (Bruker, USA), using 2 wt% $\text{DCl}/\text{D}_2\text{O}$ as a solvent for chitosan, and D_2O as solvents for the chitosan derivatives.

2.5.4. Rheology

The rheological properties of the composite inks were measured at $23\text{ }^{\circ}\text{C}$, using an Anton Paar Physica MCR 301 rheometer (Anton Paar, Austria), featuring a 25 mm diameter parallel plate geometry.

2.5.5. 3D printing

The hydrogels were printed immediately after ink preparation using



Scheme 1. Schematic representation of potential intermolecular hydrogen bonding between CNF (green), NIPU-Cys (red), and DQC (blue). (For interpretation of the references to color in this figure legend, the reader is referred to the web version of this article.)

a DIW technique with BIO-X Bioprinter (CELLINK, Sweden), equipped with a pneumatic printhead. A 3-mL clear pneumatic syringe and needle ($630\text{-}\mu\text{m}$ tip diameter) were used for printing. The printing parameters were adjusted accordingly to suit the bioprinter. Here, the gels were printed on plastic petri dishes, featuring three different patterns (round, square, and puzzle-piece shapes) and in 2 to 4 layers. The infill density was 75 %. After printing, the gels were frozen at $-18\text{ }^{\circ}\text{C}$ and dried in a vacuum oven for 24 h at $40\text{ }^{\circ}\text{C}$. The hydrogels were stored in dark and dry conditions until further use.

2.5.6. Tensile testing

Tensile testing was carried out using an Instron 4204 universal testing equipment (Instron, USA), equipped with a 100 N load cell. The average dimensions of the specimens were $L = 20\text{ mm}$; $W = 6\text{ mm}$; and $T = 1\text{ mm}$, measured with an extension speed of $10\text{ mm}/\text{min}$ at $25\text{ }^{\circ}\text{C}$. Young's modulus was calculated according to Eq. (1):

$$E = \frac{\sigma}{\varepsilon} \quad (1)$$

where σ and ε are the applied stress and subsequent strain.

2.5.7. Swelling capacity and gel content

The swelling capacity was determined following previously mentioned methods. The samples were submerged in PBS (pH 7.4) for 24 h [20]. Before submersion, the hydrogels were vacuum-dried and weighed (m_0). After 1, 3, 8, and 24 h of submersion, the samples were gently dried with tissue paper and weighed immediately (m_i). The swelling ratio was determined according to Eq. (2). The gel content was determined as the degree of crosslinking formed in the hydrogel network. The dry hydrogels were submerged in PBS for 24 h and vacuum dried at $40\text{ }^{\circ}\text{C}$ for an additional 24 h. The dry weight differences signified the cross-linked gel content percentage.

$$\text{Swelling (\%)} = \frac{m_i - m_0}{m_0} \times 100 \quad (2)$$

2.5.8. Gel stability and release of loaded DQC

The hydrolytic stability and release of loaded DQC from the hydrogels were determined *in vitro* over 8 days according to previously reported procedures [21]. The hydrogels were vacuum-dried and weighed (m_0) before being submerged in PBS (pH 7.4). The hydrogels were placed in tightly capped glass vials (in triplicate), submerged in 10 mL of PBS ($1 \times$), and stored at $37\text{ }^{\circ}\text{C}$. The samples were removed at certain time points (after 1, 3, 6, and 8 days), thoroughly vacuum-dried for 6 h, and weighed (m_j). The weight loss was calculated as an average of three tests according to Eq. (3). The gel content was determined after 1 day (24 h). FT-IR analysis of the scaffolds was conducted after 3 days to further analyze scaffold degradation and the release of loaded DQC from the matrix.

$$\text{Weight loss (\%)} = \frac{m_0 - m_j}{m_0} \times 100 \quad (3)$$

2.5.9. Scanning electron microscope (SEM)

SEM was used to examine the surface morphology of the hydrogels using a Zeiss Sigma VP Entry-level SEM (Zeiss, Germany) with an accelerating voltage of 8 kV. Additionally, SEM images of cell-seeded hydrogel scaffolds were captured after 3 days of cell culturing, using a Mira-3 SEM (TESCAN, Czech Republic), to analyze the cell adhesion/proliferation and scaffold degradation.

2.5.10. *In vitro* cytotoxicity of DQC

To estimate the optimum concentration of DQC to be incorporated into the hydrogels, the cytotoxicity of pure DQC was assessed using both direct microscopic observation and live-dead staining (FDA/PI) on cells exposed to various concentrations of DQC *in vitro*. The cytotoxicity was tested on NIH-3T3 fibroblasts, for 24 and 48 h contact times. For direct

visualization, cells were cultured in a cell culture-treated 96-well flat-bottom plate, with approximately 1×10^4 actively growing cells seeded per well with 100 μL DMEM complete medium (FBS 10 % v/v, penicillin+streptomycin). After 48 h of proliferation in a humidified CO_2 environment at 37 °C, purified DQC was dissolved in DMEM at a concentration of 20 mg/mL (stock solution), and the solution was used immediately after dissolution. The spent medium in the well was replaced with 100 μL DMEM, and 100 μL of stock solution was added and thoroughly mixed, giving an effective concentration of 10 mg/mL. Subsequent wells underwent serial dilution to achieve a concentration gradient (10, 5, 2.5, 1.25, 0.65, 0.31, and 0.15 mg/mL) for assessing the impact of DQC on cell viability and morphology. Cell visualization was conducted using an inverted microscope (Leica, Germany) at 24- and 48-h time points to observe changes in cell morphology. The tests were performed in triplicate and repeated once ($n = 6$).

For the live-dead staining assay, a similar procedure was followed, but the cells were cultured in an 8-well chamber slide (cat no. 155409, Nunc, USA). Approximately 1×10^4 actively growing NIH-3T3 cells were seeded per well with 200 μL DMEM medium and allowed to proliferate for 48 h in a humidified CO_2 environment at 37 °C. For the live-dead analysis, appropriate volumes of the DQC stock solution were added to the first well to achieve a working concentration of 2.0 mg/mL, followed by serial dilution to create a concentration gradient of 2.0, 1.0, 0.5, and 0.25 mg/mL per well. Considering the concentration and time-dependent cytotoxic effects observed in the direct visualization experiment, the 48-h time-point was considered the endpoint. After 48 h of contact time, the cells were gently washed with PBS (1 \times) before live-dead staining (FDA + PI, medium), following the manufacturer's instructions. The tests were conducted in duplicate, and imaging was carried out using a fluorescent microscope equipped with green and red filter channels (Leica, Germany).

2.5.11. Cell viability evaluation of the hydrogels

The biocompatibility of the hydrogels was assessed through an MTT cell viability assay performed on NIH-3T3 mouse fibroblasts seeded onto the scaffolds. To ensure sterility, the 3D-printed hydrogel scaffolds underwent a 1-h sterilization process in 70 % ethanol under UV light before culturing. After two washes with PBS (1 \times), the scaffolds were placed in a non-treated 24-well plate and incubated in DMEM complete medium overnight (500 μL /well). The following day, after confirming sterility, the medium was aspirated and 1×10^4 NIH-3T3 cells were seeded per scaffold, taking care to prevent cell leakage during seeding. The plates were incubated at 37 °C in 5 % CO_2 and the medium was changed every third day with 500 μL /well of fresh DMEM complete medium.

Four different hydrogels (HA-HD) were used for cell culturing, while a treated 24-well plate with no hydrogel served as a positive control group. The hydrogels were evaluated after 1, 3, 6, and 9 days of culturing, with each sample replicated four times; all tests were carried out in duplicate ($n = 8$). For the MTT assay, the scaffolds were transferred to a fresh plate and incubated with 200 μL of MTT reagent (1 mg/mL, medium) at 37 °C in 5 % CO_2 for 4 h. Following incubation, the excess medium was removed and replaced with DMSO (400 μL /well), followed by an additional 30-min incubation. Cell viability was estimated by measuring OD₅₇₀ using an Eon multi-well plate reader (BioTek Instruments, USA). Additionally, SEM images of cell-seeded scaffolds were captured after 3, 6, and 9 days of culturing NIH-3T3 cells on the scaffolds.

3. Results and discussion

In this study, we developed 3D-printable and biocompatible hydrogels consisting of quaternized chitosan (DQC), TEMPO-oxidated CNF, and non-isocyanate polyurethane (NIPU-Cys) (Scheme 1). The assessment included key parameters such as gel characterization, water absorption (swelling behavior), porosity, and elastic properties, all of paramount significance in biomedical applications. Furthermore, we

explored the impact of integrating antimicrobial DQC on the *in vitro* biocompatibility of the printed scaffolds.

3.1. FT-IR spectroscopy

FT-IR analysis was used to elucidate the chemical structure of the hydrogels (Fig. 1A). The broad band found at 3350 cm^{-1} was associated with the stretching O—H and N—H vibrations of the hydroxyl groups and the secondary amines. A strong peak at 1710 cm^{-1} and the band approximately between 2850 and 2950 cm^{-1} are likely attributed to the C=O stretching of the ester groups and the main alkane chain of the NIPU. Signals related to the C—O bonds are typically seen in the region between 1000 and 1300 cm^{-1} , thus, the peak at 1240 cm^{-1} is likely due to the C—O stretching of the esters in both NIPU and DQC. To confirm the introduction of DQC to the hydrogel matrix, a distinctive peak at 1450 cm^{-1} is likely attributed to the asymmetrical angular stretching of the methyl groups of the quaternary amine. The absorption band found at approximately 950 cm^{-1} is presumably attributed to the C—N vibrations of the quaternary ammonium groups of the chitosan. The results are consistent with previous reports [15,22]. However, due to the relatively small amounts of DQC added to the matrix and overlapping peaks, it is difficult to interpret peak contribution from individual components of the composite from FT-IR spectra alone.

3.2. Thermal properties

The thermal properties of the obtained hydrogels were studied using TGA analysis (Fig. 1B). According to the thermogram curves, the compounds exhibited large thermal degradation between 200 and 350 °C, with an approximate weight loss of 75 % for HA and a loss of approximately 65 % for the samples HB, HC, and HD. Chitosan and CNF commonly degrade in this region, due to breakage of intramolecular bonds and glycosidic linkages, leading to the degradation of the polysaccharide structure itself [23].

3.3. DIW printing and rheological analysis

3D printable hydrogels are beneficial in various biomedical applications, such as wound-healing dressings tailored for irregularly shaped wounds, ranging from burn injuries to deep chronic wounds. DIW is a 3D printing method particularly suitable for temperature-sensitive materials, however, specific rheological requirements are necessary for ideal printing [24]. To enhance the rheological properties and printability of the hydrogel inks, TEMPO-oxidated CNF was incorporated into the matrix. The resultant gel network is based on hydrogen bonding interactions between its constituents (Scheme 1).

As depicted in Fig. 2A, the inks exhibited very high viscosity at low shear rates that sharply decreased at higher shear rates. This phenomenon is attributed to the disruption of relatively weak hydrogen bonds within the matrix, leading to a loss of network architecture. This observation signifies the formation of secondary hydrogen bonding responsible for network formation, contributing to a distinctive reversible shear-thinning behavior. This behavior holds significant relevance in 3D printing applications, where the rapid restoration of the ink's viscous behavior is crucial for both the printability and dimensional accuracy of the printed structures. Furthermore, the noticeable cross-over points, located at approximately 150–170 Pa (Fig. 2B), indicate a rapid sol-gel transition at relatively low shear rates. Importantly, the gel formation process lacks chemical cross-linking, with hydrogen bonds forming rapidly at the identified cross-over points (Fig. 2B-inset). These findings emphasize the complex yet crucial interaction of rheological dynamics governing shear-thinning behavior and rapid gelation. Ultimately, these results affirm the suitability of the developed hydrogel inks for DIW applications.

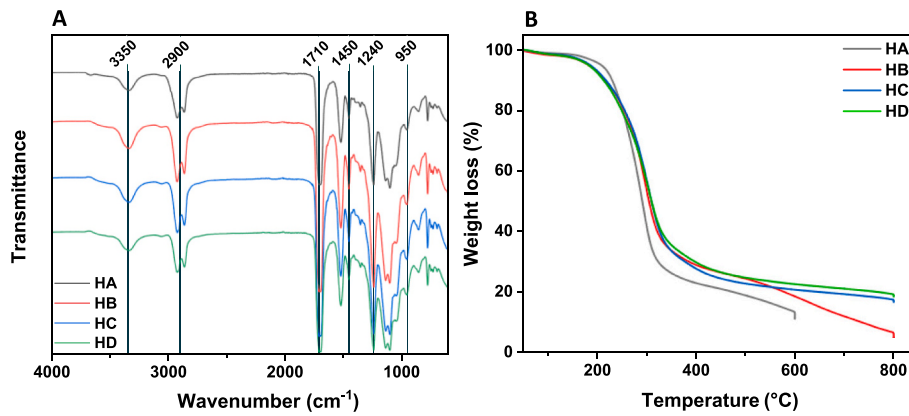


Fig. 1. (A) FT-IR spectra; and (B) TGA curves of the obtained hydrogel scaffolds.

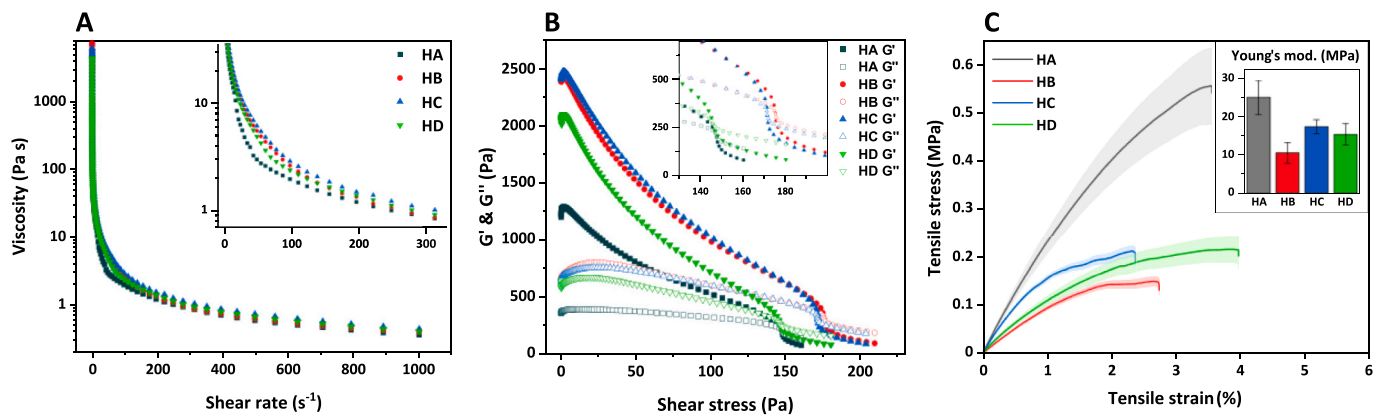


Fig. 2. Rheological and mechanical characterization of the inks and obtained hydrogel scaffolds. (A) Viscosity flow curves, and (B) rheological properties (storage (G') and loss (G'') moduli) of the inks. (C) Mechanical properties of the 3D printed dried hydrogel scaffolds: stress-strain curves and Young's modulus of the dried scaffolds (inset). [$n = 3$, average \pm SD].

3.4. Mechanical properties

The hydrogel without DQC (HA) displayed higher stiffness and strength compared to the hydrogels containing DQC (Fig. 2C). The differences between HB-HD were minor, although HB showed the least

favorable mechanical properties. The introduction of chitosan led to a reduction in the mechanical characteristics of the hydrogels in a dry state, presumably due to the alteration of the uniform internal structure of NIPU and CNF (Fig. 4A) [25,26]. An increase in the porous structure in the hydrogels was associated with a weakened mechanical

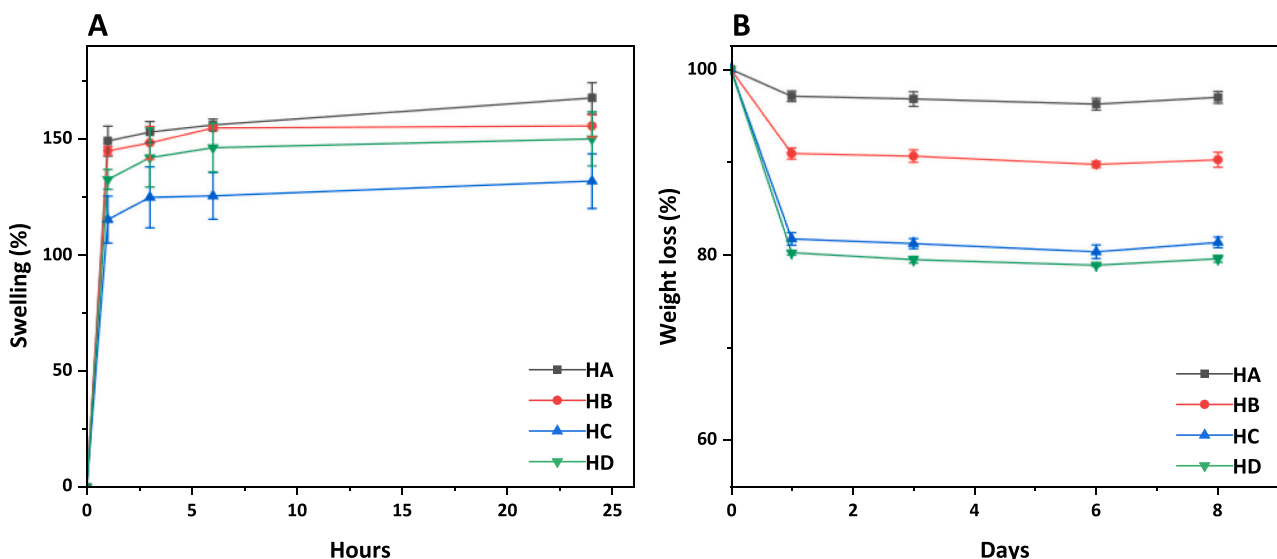


Fig. 3. (A) Swelling ratio and (B) degradation of the hydrogels submerged in PBS. [$n = 3$, average \pm SD].

performance. The Young's modulus, representing the relationship between the applied force and the resulting deformation of the hydrogel, is depicted in Fig. 2C(inset) and in (Table S2). Among the hydrogels, HA exhibited the highest Young's modulus, followed by HC. The incorporation of DQC disrupted the otherwise orderly tightly packed network, presumably increasing porosity and consequently lowering the values of Young's moduli [27]. However, the differences among the hydrogels containing DQC were minor.

3.5. Swelling capacity and gel stability

Swelling capacity is one of the most important characteristics of hydrogels. Despite the water solubility of quaternized chitosan, the obtained hydrogels did not dissolve nor disintegrate in water, indicating a successful cross-linked network establishment. The water absorption capacity (Fig. 3A) stabilized after 1–2 h and the hydrogels exhibited weight gain ranging from 130 % to 160 %. Both DQC and CNF possess good swelling properties owing to the strong hydrogen bonding between the polysaccharides and water molecules [28]. PUs typically exhibit poorer water retention properties due to their chemical structure and hydrophobic nature. However, the synthesized NIPUs incorporate hydrophilic components, introducing hydroxyl groups and thereby enhancing the polymer's swelling behavior [29]. No significant differences were observed among the four hydrogel composites (Fig. 3A), although, with an increasing amount of DQC in the matrix, the swelling was slightly reduced. Complex structures with branching and side chains influence the swelling characteristics, we presume that the addition of DQC interrupts the linear structure of the polymer matrix and therefore slightly reduces the swelling of the material.

Fig. 3B depicts the hydrolytic stability of the hydrogels over 8 days, revealing a noticeable weight loss within the initial 24 h that subsequently stabilizes. The initial weight loss is presumably due to unreacted units and free uncross-linked fractions of the various components, which were washed away upon submersion in PBS. FT-IR spectroscopy conducted after 3 days of submersion (Fig. S3) indicated a uniform release of hydrogel components rather than the exclusive loss of specific elements. Observations through FT-IR (Fig. S3) revealed that only a fraction of DQC got released during the initial washing, while the rest remained embedded in the hydrogel matrix, which gradually got released from the slowly swelling hydrogels, providing a sustained release. The gel content was determined after 24 h of incubation as 97, 91, 82, and 80 %, for the hydrogels HA-HD, respectively. By increasing the amount of DQC in the hydrogel, the weight loss increased, and the gel content decreased. This is presumably attributed to the more

compact and linear structure of HA, giving it a stronger cross-linked network, whereas the addition of DQC interrupts this orderly network.

3.6. SEM analysis

SEM imaging was used to investigate the surface and the internal morphology of the hydrogel cross-section (Fig. 4). The hydrogels exhibited a porous structure attributed to the presence of CNF and DQC, a favorable feature for facilitating moisture control in hydrogels. Furthermore, the images revealed a uniform morphology, indicating excellent compatibility among the components.

3.7. *In vitro* cytotoxicity of DQC

An increase in cytotoxicity with increasing concentration raises significant concerns when considering applications of quaternary chitosan, particularly in medical contexts such as *in vivo* applications. According to studies, this behavior is dependent on the degree of quaternization and the molecular weight of the components [30]. The amount of incorporated DQC in the hydrogels should be determined by the balance between achieving the highest antibacterial activity [15,31,32] and maintaining the lowest possible cytotoxicity. The cytotoxicity assessment of the synthesized DQC was conducted on NIH-3T3 fibroblasts, for 24- or 48-h contact times at various concentrations (Fig. 5A, Fig. S4). For a 48-h contact time, the DQC demonstrated an LD50 of approximately 0.5 mg/mL. Below this concentration, the cytotoxicity markedly diminished, as observed through direct microscopic observation of the cells. At a DQC concentration of 0.62 mg/mL, the cells exhibited a morphology similar to the control cells, with only a few cells displaying altered morphology. This change was even less pronounced at 0.31 mg/mL. Quantifying the live-dead analysis (Fig. 5B, Fig. S4) revealed a significantly higher number of dead cells (yellow/red) at 1 mg/mL (≈ 85 % dead) compared to ≈ 60 % at 0.5 mg/mL. Below this concentration, the toxicity was negligible, as the viability approached 80 % at 0.25 mg/mL DQC.

3.8. *In vitro* biocompatibility analysis

The overall biocompatibility assessment of the 3D-printed hydrogel scaffolds was determined with an MTT assay, evaluating the impact of DQC concentration in the hydrogels (HA-HD). The *in vitro* biocompatibility was evaluated using NIH-3T3 fibroblast cells after 1, 3, 6, and 9 days of growth, with analysis focused on the metabolic activity of the cells (Fig. 5C, Fig. S5). Throughout the test duration, the cells exhibited

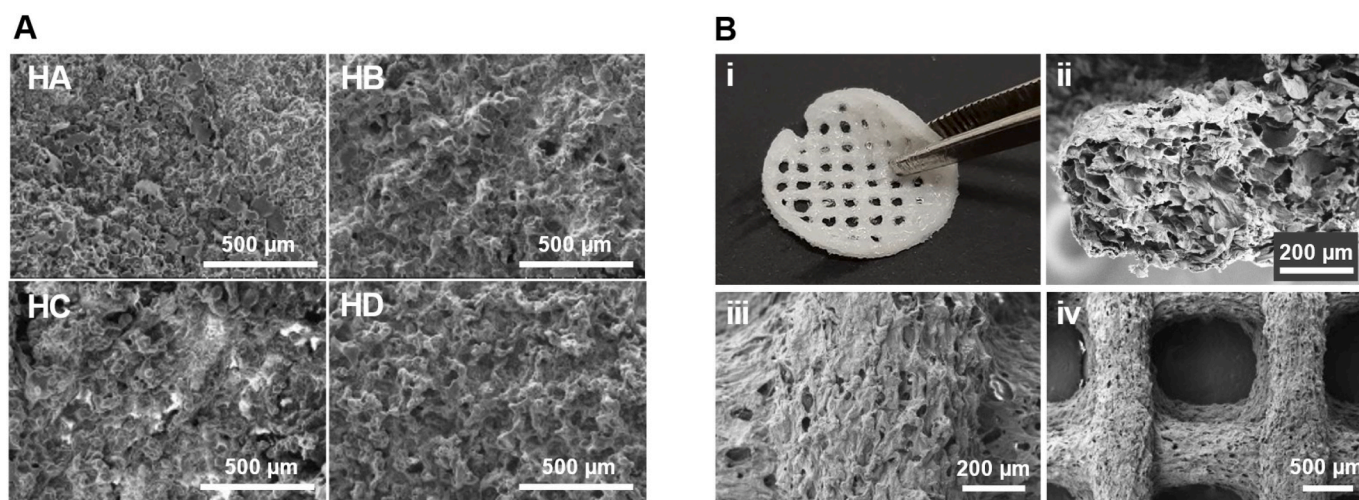


Fig. 4. (A) SEM images of HA-HD hydrogels showing the surface topology and porous structures. (B) Hydrogel HD: (i) digital photography demonstrating its flexibility, and (ii-iv) SEM images showing the cross-sectional and surface morphology of the hydrogel.

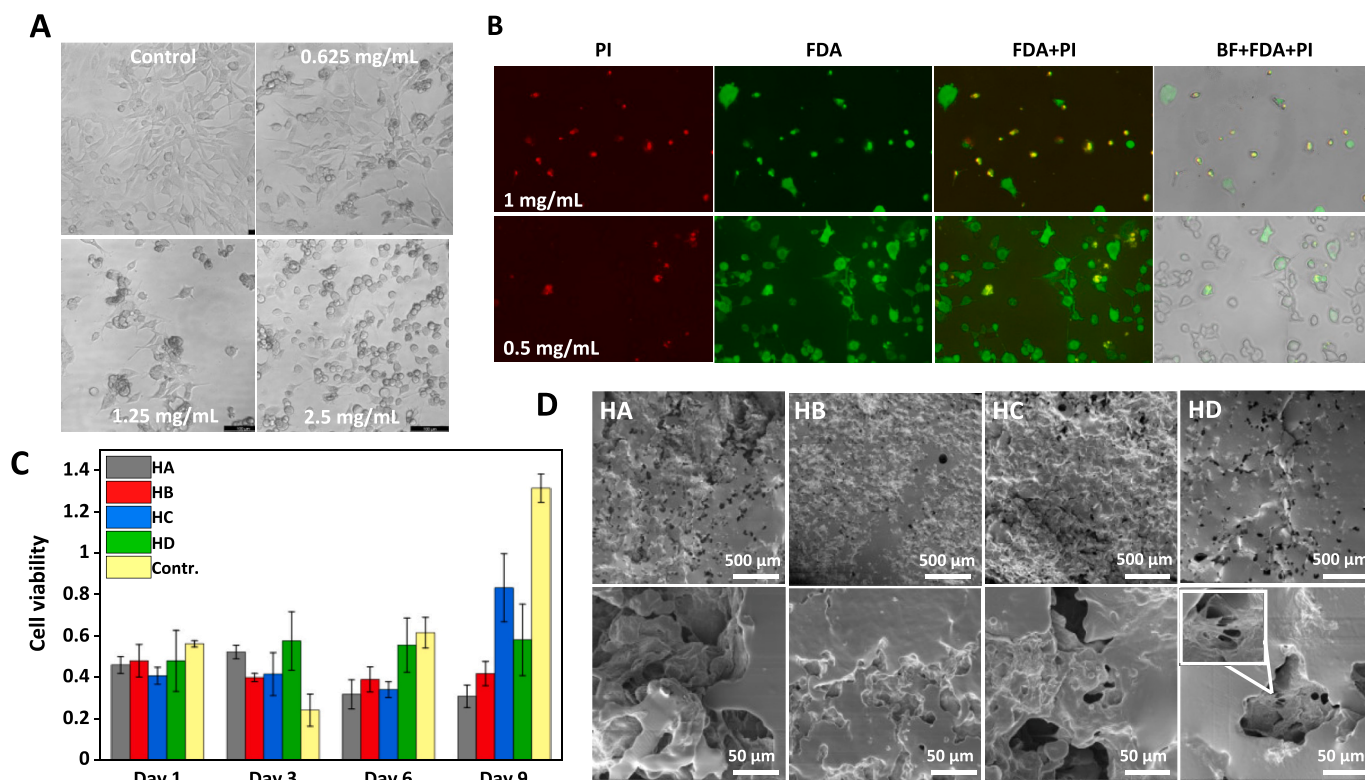


Fig. 5. Cell viability and biocompatibility studies; (A) microscopic images showing cell morphology at various DQC concentrations after 48 h of contact time, and (B) live-dead assay showing live (green) and dead (yellow/red) cells, at various DQC concentrations after a 48-h contact time. (C) Quantitative cell viability evaluation of the hydrogel scaffolds (HA-HD) via an MTT assay, and (D) SEM images of NIH-3T3 cells growing on the hydrogel scaffolds after 3 days of cultivation. (For interpretation of the references to colour in this figure legend, the reader is referred to the web version of this article.)

no acute toxicity and remained viable on the scaffold surface. However, cell proliferation on the scaffold surface was slower compared to the control surface (cell-culture treated). Notably, higher DQC concentrations in the scaffolds, specifically HC and HD, resulted in increased cell proliferation activity. Conversely, the HA hydrogel exhibited the lowest overall cell proliferation, indicating a bioinert surface of the NIPU-Cys with limited cell adhesion and proliferation activity. This is aligned with the hypothesis that the inclusion of quaternary chitosan would enhance the hydrogel biocompatibility [33]. Low adhesion is advantageous for applications like wound dressings, preventing adherence to newly formed fragile skin, facilitating easy removal, and minimizing tissue injury during dressing replacements. Here, HC demonstrated the highest cell viability after 9 days, though the overall cell viability of HC and HD were quite similar. Despite containing the highest amount of DQC, the reduced viability in HD may be attributed to greater degradation and consequently, a lower amount of DQC in the hydrogel structure. SEM images of the scaffolds taken after 3, 6, and 9 days of cell cultivation revealed a porous scaffold architecture (Fig. 5D, Fig. S6). With a limited number of cells on the scaffold's surface, uniform growth was not observed. Instead, cells appeared to concentrate at specific focal points and within cavities, possibly due to the localized presence of CNF and DQC, providing anchoring surfaces (Fig. 5D).

Considering the quantities of DQC integrated into the hydrogels and the outcome of the cell viability assay, along with the static environment conditions in the assays, the cell cytotoxicity of pure DQC was not concluded as a definite factor. The context of the intended application becomes crucial when assessing cytotoxicity. The primary goal of this work was to develop a hydrogel intended to function as a protective intermediary layer between the primary wound dressing and its external surroundings. Given the recognized slightly toxic tendencies of DQC, direct contact between the hydrogel layer and live tissue was intentionally limited. Conversely, the hydrogels are designed to serve as an

effective protective barrier against pathogenic microbes settling on the wound's surface. The porous and hydrophilic nature of the hydrogels will facilitate excellent absorption of wound exudates and provide a moist environment at the wound site, promoting favorable conditions for wound healing.

However, to comprehensively explore the biomedical possibilities of the hydrogels and gain a deeper understanding of their activity, future studies should involve *in vivo* experiments. Such experiments, though outside the scope of this project, are crucial for a thorough assessment. Our focus in this project was on a preliminary proof-of-concept, involving comprehensive material characterization and 3D printability assessments while targeting activity and cytotoxicity through *in vitro* studies.

4. Conclusion

In this research, we have successfully synthesized and characterized biocompatible and antibacterial hydrogels, composed of DQC, NIPU-Cys, and TEMPO-CNF. The primary objective was to evaluate the hydrogel's properties, assess ink printability, and investigate the impact of varying DQC concentrations on both biocompatibility and overall physiochemical attributes. The aim was to formulate a hydrogel capable of serving as an effective biocompatible barrier layer for biomedical applications. The incorporation of DQC had minor effects on the ink printability and the mechanical properties of the hydrogel scaffolds, presumably due to the interruption of the otherwise orderly network. Furthermore, the hydrogel inks exhibited favorable shear-thinning behavior coupled with efficient and rapid gelation, rendering them well-suited for DIW 3D printing. The hydrogels exhibited good swelling ratios and porous architecture, making them particularly suitable for applications like wound management. Importantly, the introduction of DQC enhanced *in vitro* cell proliferation on the scaffolds without

negatively impacting the viability. This indicates that the slightly cytotoxic tendencies of quaternary chitosan diminish when it is present in an NIPU-CNF matrix. Based on these outcomes, the combination of DQC in a NIPU-Cys-CNF matrix emerges as a promising composition for crafting 3D-printable, biocompatible, and porous hydrogels with excellent swelling properties. These materials hold significant potential as constituents for creating biocompatible materials for various biomedical applications.

CRedit authorship contribution statement

Isabella Laurén: Writing – review & editing, Writing – original draft, Methodology, Investigation, Formal analysis, Conceptualization. **Afsoon Farzan:** Writing – review & editing, Writing – original draft, Methodology, Investigation, Formal analysis, Conceptualization. **Arun Teotia:** Writing – review & editing, Writing – original draft, Methodology, Investigation, Formal analysis. **Nina C. Lindfors:** Writing – review & editing, Writing – original draft. **Jukka Seppälä:** Writing – review & editing, Supervision, Funding acquisition, Conceptualization.

Declaration of generative AI and AI-assisted technologies in the writing process

During the preparation of this work, the authors used ChatGPT 3.5 to improve the language. After using this service, the authors reviewed and edited the content as needed and take full responsibility for the content of the publication.

Declaration of competing interest

No conflicts to declare.

Acknowledgments

The authors would like to thank Svenska Kulturfonden, Magnus Ehrnrooth Foundation, and the Finnish Cultural Foundation for providing funding and Ph.D. scholarships. This work made use of BIO-ECONOMY infrastructure at Aalto University.

Appendix A. Supplementary data

Reaction schemes of chitosan derivatives (Scheme S1); FT-IR and NMR spectra of chitosan derivatives (Fig. S1); FT-IR and NMR spectra of NIPU-Cys (Fig. S2); FT-IR spectra after degradation (Fig. S3); Cell morphology and live/dead analysis (Fig. S4); Cell viability assay (Fig. S5); SEM images (Fig. S6); TGA data (Table S1); Mechanical properties (Table S2). Supplementary data to this article can be found online at <https://doi.org/10.1016/j.ijbiomac.2024.129321>.

References

- [1] S.J. Buwalda, K.W.M. Boere, P.J. Dijkstra, J. Feijen, T. Vermonden, W.E. Hennink, Hydrogels in a historical perspective: from simple networks to smart materials, *J. Control. Release* 190 (2014) 254–273, <https://doi.org/10.1016/j.jconrel.2014.03.052>.
- [2] T. Vermonden, B. Klumperman, The past, present and future of hydrogels, *Eur. Polym. J.* 72 (2015) 341–343, <https://doi.org/10.1016/j.eurpolymj.2015.08.032>.
- [3] H. Hamed, S. Moradi, S.M. Hudson, A.E. Tonelli, Chitosan based hydrogels and their applications for drug delivery in wound dressings: a review, *Carbohydr. Polym.* 199 (2018) 445–460, <https://doi.org/10.1016/j.carbpol.2018.06.114>.
- [4] C. Viezzer, R. Mazzuca, D.C. Machado, M.M. de Camargo Forte, J.L. Gómez Ribelles, A new waterborne chitosan-based polyurethane hydrogel as a vehicle to transplant bone marrow mesenchymal cells improved wound healing of ulcers in a diabetic rat model, *Carbohydr. Polym.* 231 (2020) 115734, <https://doi.org/10.1016/j.carbpol.2019.115734>.
- [5] E. Rezvani Ghomi, S. Khalili, S. Nouri Khorasani, R. Esmaeeli Neisiany, S. Ramakrishna, Wound dressings: current advances and future directions, *J. Appl. Polym. Sci.* 136 (2019) 1–12, <https://doi.org/10.1002/app.47738>.
- [6] X. Qing, G. He, Z. Liu, Y. Yin, W. Cai, L. Fan, et al., Preparation and properties of polyvinyl alcohol/N-succinyl chitosan/lincomycin composite antibacterial hydrogels for wound dressing, *Carbohydr. Polym.* (2021) 261, <https://doi.org/10.1016/j.carbpol.2021.117875>.
- [7] J. Joseph, R.M. Patel, A. Wenham, J.R. Smith, Biomedical applications of polyurethane materials and coatings, *Trans. Inst. Met. Finish.* 96 (2018) 121–129, <https://doi.org/10.1080/00202967.2018.1450209>.
- [8] L. Maisonneuve, O. Lamarzelle, E. Rix, E. Grau, H. Cramail, Isocyanate-free routes to polyurethanes and poly(hydroxy urethane)s, *Chem. Rev.* 115 (2015) 12407–12439, <https://doi.org/10.1021/acs.chemrev.5b00355>.
- [9] A. Gomez-Lopez, F. Elizalde, I. Calvo, H. Sardon, Trends in non-isocyanate polyurethane (NIPU) development, *Chem. Commun.* 57 (2021) 12254–12265, <https://doi.org/10.1039/d1cc05009e>.
- [10] A. Farzan, S. Borandeh, N. Zanjanzadeh Ezazi, S. Lipponen, H.A. Santos, J. Seppälä, 3D scaffolding of fast photocurable polyurethane for soft tissue engineering by stereolithography: influence of materials and geometry on growth of fibroblast cells, *Eur. Polym. J.* (2020) 139, <https://doi.org/10.1016/j.eurpolymj.2020.109988>.
- [11] H. Liu, C. Wang, C. Li, Y. Qin, Z. Wang, F. Yang, et al., A functional chitosan-based hydrogel as a wound dressing and drug delivery system in the treatment of wound healing, *RSC Adv.* 8 (2018) 7533–7549, <https://doi.org/10.1039/c7ra13510f>.
- [12] R. Jayakumar, M. Prabaharan, P.T. Sudheesh Kumar, S.V. Nair, H. Tamura, Biomaterials based on chitin and chitosan in wound dressing applications, *Biotechnol. Adv.* 29 (2011) 322–337, <https://doi.org/10.1016/j.biotechadv.2011.01.005>.
- [13] S.J. Buwalda, Bio-based composite hydrogels for biomedical applications, *Multifunctional Materials* (2020) 3, <https://doi.org/10.1088/2399-7532/ab80d6>.
- [14] B.I. Andreica, X. Cheng, L. Marin, Quaternary ammonium salts of chitosan. A critical overview on the synthesis and properties generated by quaternization, *Eur. Polym. J.* (2020) 139, <https://doi.org/10.1016/j.eurpolymj.2020.110016>.
- [15] A. Teotia, I. Laurén, S. Borandeh, J. Seppälä, Quaternized chitosan derivatives as viable antiviral agents: structure-activity correlations and mechanisms of action, *ACS Appl. Mater. Interfaces* 15 (2023) 18707–18719, <https://doi.org/10.1021/acsami.3c01421>.
- [16] S. Borandeh, I. Laurén, A. Teotia, J. Niskanen, J. Seppälä, Dual functional quaternary chitosans with thermoresponsive behavior: structure-activity relationships in antibacterial activity and biocompatibility, *J. Mater. Chem. B* (2023), <https://doi.org/10.1039/D3TB02066E>.
- [17] H. Baniasadi, R. Ajdary, J. Trifol, O.J. Rojas, J. Seppälä, Direct ink writing of aloe vera/cellulose nanofibrils bio-hydrogels, *Carbohydr. Polym.* (2021) 266, <https://doi.org/10.1016/j.carbpol.2021.118114>.
- [18] A. Farzan, S. Borandeh, H. Baniasadi, J. Seppälä, Environmentally friendly polyurethanes based on non-isocyanate synthesis, *Express Polym Lett* 18 (2024) 88–101, <https://doi.org/10.3144/expresspolymlett.2024.7>.
- [19] H. Baniasadi, R. Ajdary, J. Trifol, O.J. Rojas, J. Seppälä, Direct ink writing of aloe vera/cellulose nanofibrils bio-hydrogels, *Carbohydr. Polym.* (2021) 266, <https://doi.org/10.1016/j.carbpol.2021.118114>.
- [20] H. Baniasadi, Z. Madani, R. Ajdary, O.J. Rojas, J. Seppälä, Ascorbic acid-loaded polyvinyl alcohol/cellulose nanofibril hydrogels as precursors for 3D printed materials, *Materials Science and Engineering C* (2021) 130, <https://doi.org/10.1016/j.msec.2021.112424>.
- [21] G. Janarthanan, H.N. Tran, E. Cha, C. Lee, D. Das, I. Noh, 3D printable and injectable lactoferrin-loaded carboxymethyl cellulose-glycol chitosan hydrogels for tissue engineering applications, *Mater. Sci. Eng. C* (2020) 113, <https://doi.org/10.1016/j.msec.2020.111008>.
- [22] K.Y. Chen, S.Y. Zeng, Fabrication of quaternized chitosan nanoparticles using tripolyphosphate/genipin dual cross-linkers as a protein delivery system, *Polymers (Basel)* (2018) 10, <https://doi.org/10.3390/polym10111226>.
- [23] A. Sarwar, H. Katas, S.N. Samsudin, N.M. Zin, Regioselective sequential modification of chitosan via azide-alkyne click reaction: synthesis, characterization, and antimicrobial activity of chitosan derivatives and nanoparticles, *PLoS One* (2015) 10, <https://doi.org/10.1371/journal.pone.0123084>.
- [24] M.A.S.R. Saadi, A. Maguire, N.T. Pottackal, M.S.H. Thakur, M.M. Ikram, A.J. Hart, et al., Direct ink writing: a 3D printing technology for diverse materials, *Adv. Mater.* 34 (2022) 1–57, <https://doi.org/10.1002/adma.202108855>.
- [25] A. Piotrowska-Kirschling, J. Brzeska, The effect of chitosan on the chemical structure, morphology, and selected properties of polyurethane/chitosan composites, *Polymers (Basel)* 12 (2020) 1205, <https://doi.org/10.3390/polym12051205>.
- [26] D.Y. Zuo, Y.Z. Tao, Y.B. Chen, W.L. Xu, Preparation and characterization of blend membranes of polyurethane and superfine chitosan powder, *Polym. Bull.* 62 (2009) 713–725, <https://doi.org/10.1007/s00289-009-0049-8>.
- [27] F. You, X. Wu, X. Chen, 3D printing of porous alginate/gelatin hydrogel scaffolds and their mechanical property characterization, *Int. J. Polym. Mater. Polym. Biomater.* 66 (2017) 299–306, <https://doi.org/10.1080/00914037.2016.1201830>.
- [28] J. Torstensen, M. Liu, S.A. Jin, L. Deng, A.I. Hawari, K. Syverud, et al., Swelling and free-volume characteristics of TEMPO-oxidized cellulose nanofibril films, *Biomacromolecules* 19 (2018) 1016–1025, <https://doi.org/10.1021/acs.biomac.7b01814>.
- [29] J.J. Warner, P. Wang, W.M. Mellor, H.H. Hwang, J.H. Park, S.H. Pyo, et al., 3D printable non-isocyanate polyurethanes with tunable material properties, *Polym. Chem.* 10 (2019) 4665–4674, <https://doi.org/10.1039/c9py00999j>.
- [30] A. Zubareva, B. Shagdarova, V. Varlamov, E. Kashirina, E. Svirshchevskaya, Penetration and toxicity of chitosan and its derivatives, *Eur. Polym. J.* 93 (2017) 743–749, <https://doi.org/10.1016/j.eurpolymj.2017.04.021>.
- [31] M.M. Hassan, Enhanced antimicrobial activity and reduced water absorption of chitosan films graft copolymerized with poly(acryloyloxy)

- ethyltrimethylammonium chloride, *Int. J. Biol. Macromol.* 118 (2018) 1685–1695, <https://doi.org/10.1016/j.ijbiomac.2018.07.013>.
- [32] P. Sahariah, M. Måsson, Antimicrobial chitosan and chitosan derivatives: a review of the structure-activity relationship, *Biomacromolecules* 18 (2017) 3846–3868, <https://doi.org/10.1021/acs.biomac.7b01058>.
- [33] E.D. Freitas, C.F. Moura, J. Kerwald, M.M. Beppu, An overview of current knowledge on the properties, synthesis and applications of quaternary chitosan derivatives, *Polymers (Basel)* 12 (2020) 1–41, <https://doi.org/10.3390/polym12122878>.